Article

Advances in Additive Friction Extrusion Deposition (AFED): Process and Tool Design

Max Hossfeld [1,2,*] and Arnold Wright [3]

1 InnovationCampus Future Mobility, University of Stuttgart, Nobelstraße 15, 70569 Stuttgart, Germany
2 fsw.expert GmbH, Breiter Weg 1, 72622 Nürtingen, Germany
3 Bond Technologies, 1353 Wade Drive, Suite B, Elkhart, IN 46514, USA; arnold.wright@bondtechnologies.net
* Correspondence: max.hossfeld@ifsw.uni-stuttgart.de

Abstract: Additive friction extrusion deposition (AFED) is a recently developed additive manufacturing technique that promises high deposition rates at low forces. Due to the novelty of the process, the underlying phenomena and their interactions are not fully understood, and in particular, the processing strategy and tool design are still in their infancy. This work contributes to the state-of-the-art of AFED through a comprehensive analysis of its working principles and an experimental program, including a representative sample component. The working principle and process mechanics of AFED are broken down into their individual components. The forces and their origins and effects on the process are described, and measures of process efficiency and theoretical minimum energy consumption are derived. Three geometrical features of the extrusion die were identified as most relevant to the active material flow, process forces, and deposition quality: the topography of the inner and outer circular surfaces and the geometry of its extrusion channels. Based on this, the experimental program investigated seven different tool designs in terms of efficiency, force reduction, and throughput. The experiments using AA 6061-T6 as feedstock show that AFED is capable of both high material throughput (close to $550\,\text{mm}^3/\text{s}$) and reduced substrate forces, for example, the forces for a run at $100\,\text{mm}^3/\text{s}$ remained continuously below $500\,\text{N}$ and for a run at $400\,\text{mm}^3/\text{s}$ below $3500\,\text{N}$. The material flow and microstructure of AFED were assessed from macro-sections. Significant differences were found between the advancing and retracting sides for both process effects and material flow. Banded structures in the microstructure show strong similarities to other solid-state processes. The manufacturing of the sample components demonstrates that AFED is already capable of producing industrial-grade components. In mechanical tests, interlayer bonding defects resulted in more brittle failure behavior in the build direction of the structure, whereas in the horizontal direction, mechanical properties corresponding to a T4 temper were achieved.

Keywords: FSAM; AFED; additive manufacturing; aluminum; tool design; process optimization

1. Introduction

Solid-state additive manufacturing offers several advantages over other additive manufacturing (AM) technologies [1–6]. Of particular note are the following:

- Very low energy input and consumption;
- The utilization of inexpensive, easily available feedstock;
- Nn melting of the materials involved,;
- Excellent mechanical properties;
- The possibility of joining different materials such as steel/aluminum.

Other increasingly important benefits in terms of environmental objectives include the direct recycling of material normally considered waste, such as machine chips [3], and the possibility of high-quality part repair [5,7]. The main disadvantages of friction-based solid-state additive processes are the comparatively high process forces stemming from their solely mechanical working principles [8]. These forces must be supported by the

substrate and subsequently by the structure of the build. This limits the manufacture of thin or weak structures since the process requires a certain degree of stability and stiffness, i.e., a minimum wall of built structures.

In this context, additive friction extrusion deposition (AFED) [6], a recently developed additive manufacturing process, offers the opportunity to combine the benefits of solid-state processing while having several advantages in reducing the mechanical and thermal impact on both the substrate and the built structure. This paper contributes to the knowledge and state-of-the-art of AFED by offering the following:

- A detailed description of the basic principles of the process;
- An identification and assessment of AFED process mechanics;
- An analysis of steady-state process conditions;
- Recommendations for the design and optimization of the process, i.e., parameter selection and tool design;
- A characterization of material flow, the resulting microstructure, and the correlating mechanical properties;
- A review of the current technology readiness level (TRL) of the process.

After a full analysis of the working principles of AFED, the results of an experimental program are presented. Seven tool designs were investigated. Based on the results of this examination, a representative sample component was built and evaluated by metallography and tensile testing.

2. Process Fundamentals

AFED involves the thermo-mechanical plastification of feedstock within a rotating spindle and its subsequent extrusion and deposition onto a substrate. The AFED process starts with the feedstock being contained inside a nonrotating guide tube that is located inside a rotating spindle, Figure 1. The upper end of the guide tube contains a push rod that can force the feedstock material downwards with a defined velocity or force. The lower end of the guide tube is covered by an extrusion die that is mounted on the spindle. As this die rotates with the spindle and the nonrotating feedstock is pressed against it, the lower end of the feedstock is plasticized through frictional heating, plastic work dissipation, and shearing [9].
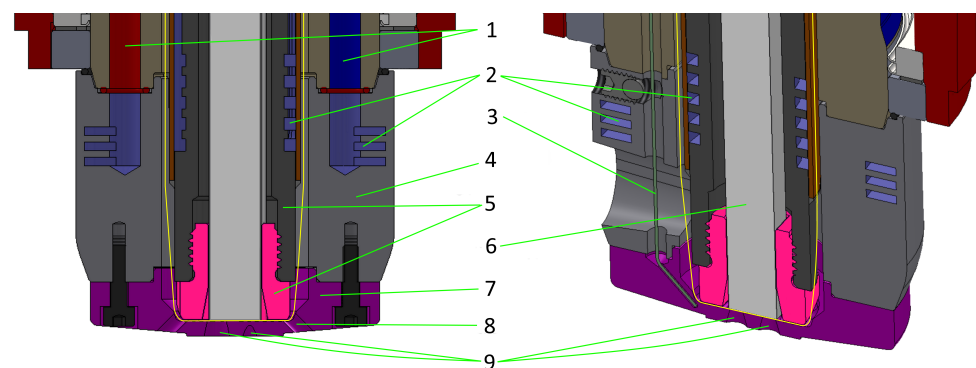

Figure 1. Cross-sections of AFED tooling: (1) coolant supply and return; (2) coolant passages; (3) thermocouple; (4) die holder; (5) guide tube with lower end (pink); (6) feedstock; (7) extrusion die; (8) outlet passages for material overflow to the sides; (9) extrusion channels. Note: all parts besides (5) and (6) rotate during the process (separation indicated by yellow line).

Subsequently, the material is forced (extruded) through the die. As the outer surface of the die is positioned at a suitable height above a substrate, the material being extruded is contained between the die and the substrate. Here, additional heating and mixing occurs, bonding the extruded material to the substrate. As the spindle is moved along a path in the x, y, and z axes, a 3D structure is created. Typical measures known from other solid-state processes may be applied to further influence the AFED process. For instance, both the

spindle and the guide tube may be cooled (or heated) to influence the temperature of the deposited material or to reduce the binding of the feedstock to the guide tube.

2.1. The Essential Forces of AFED and Their Origin

An overview of the most relevant forces involved in the AFED process is given in Figure 2. These forces can be divided into two main categories: *inner* and *outer* forces. The *inner forces* involved in initially plasticizing the feedstock (M_{inner}, F_f), and are reacted to within the tooling and do not reach the substrate. The *outer forces* (M_{outer}, F_s) are caused by the deposition process, and they act between the outer surface of the extrusion die and the substrate. When the AFED process starts, the feedstock has not yet been deformed and is at ambient temperature. In the start-up phase, the only forces acting are M_{inner} and F_f. However, as the feedstock is plasticized and moved through the extrusion die, M_{outer} and F_s start to rise as soon as the material is constrained against the substrate. This provides additional heat input into the process while, at the same time, causing conduction through the substrate to provide a further heat sink. The relationship between the material flow volume (determined by feed velocity, v_f, and die design), layer height, h_{layer}, and the traverse velocity, v_t, determines the resulting layer width. Of course, this width of the extruded layer has a natural upper limit that is approximately the width of the outer structures of the die, see Figure 2.
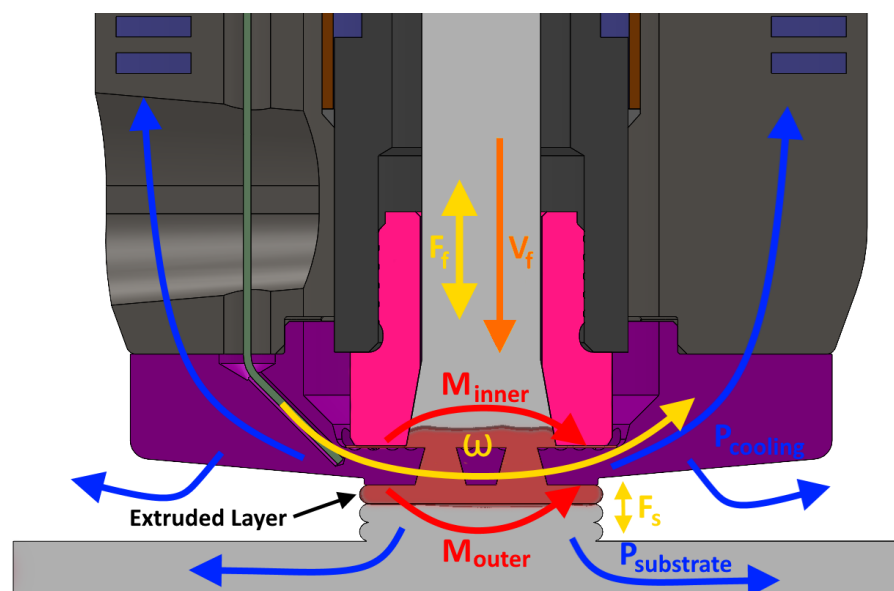
Figure 2. Overview of the most relevant forces in the process and illustration of material flow, heat generation, the AFED process (red), and dissipation into the build and periphery (blue).

2.2. Energy Balance and Efficiency

The measured spindle power does not directly correspond to the power going into the deposited material, as there are several power sources and sinks. The power sources include the spindle power, the rod feeder power, and the surface drag as the tooling moves along the tool path. The power sinks include the energy to heat the material, the work to actually deform the material, heat lost to the substrate, and heat lost to tool cooling. These sinks can be characterized as the minimum energy for the process plus losses due to cooling. The overall energy flow can, therefore, be expressed as the following equation:

$$P_{spindle} + P_{rodfeed} + P_{traverse} = P_{heating} + P_{deformation} + P_{losses} \tag{1}$$

The spindle power, $P_{spindle}$, can be split thus:

$$P_{spindle} = P_{inner} + P_{outer} \tag{2}$$

$$= \omega \cdot (M_{inner} + M_{outer}) \tag{3}$$

The power input from the rod feeder can be calculated from the rod force and velocity:

$$P_{rodfeeder} = F_f \cdot V_f \tag{4}$$

Finally, the energy input from the tool moving across the surface is calculated thus:

$$P_{traverse} = F_{traverse} \cdot V_{traverse} \tag{5}$$

The P_{losses} on the other side of Equation (1) are more difficult to calculate, which is also true for $P_{deformation}$. However, $P_{heating}$ can be determined using the material properties:

$$P_{heating} = \dot{m}_{material} \cdot c_{p,material} \cdot \Delta T \tag{6}$$

With this, there are two different measures of efficiency that could reasonably be calculated for the AFED process: one being the efficiency of the depositing material $\eta_{deposit}$ with respect to the minimum energy required, and the other being the absolute energy used to deposit a defined amount of material, $e_{process}$:

$$\eta_{deposit} = \frac{P_{heating} + P_{deformation}}{P_{heating} + P_{deformation} + P_{losses}} \qquad [1] \tag{7}$$

$$e_{process} = \frac{P_{heating} + P_{deformation} + P_{losses}}{\dot{m}_{material}} \qquad [\text{J/kg}] \tag{8}$$

$$= \frac{P_{spindle} + P_{rodfeed} + P_{traverse}}{\dot{m}_{material}} \qquad [\text{J/kg}] \tag{9}$$

While $\eta_{deposit}$ would be a good indicator of the absolute efficiency of the process, it is difficult to determine both $P_{deformation}$ and P_{losses}. The value of $\eta_{deposit}$ is greatly affected by the estimates used for these values, reducing its value as an indicator. However, the values for the $e_{process}$, as given in Equation (9), are all directly measurable or easily calculated, and therefore, $e_{process}$ was chosen as the preferred criterion for process efficiency for later analysis. Another benefit is that specific energy consumption is often reported in other publications, allowing for direct comparability with other deposition processes. The best $e_{process}$ is as small as possible and relates to $\eta_{deposit}$ through the following equation:

$$\eta_{deposit} = \frac{e_{process(theoretical\ miniumum)}}{e_{process(observed)}} \tag{10}$$

While it is not the aim of this work to assess the ideal $e_{process(theoretical\ miniumum)}$, it can be derived that it must be lower than 6 GJ/t from the experiments represented in Figure 8.

3. Material

3.1. Feedstock and Substrate: Material and Properties

The feedstock used for this study was a square bar rod with dimensions of 12.7 mm × 12.7 mm × 305 mm. Plates of dimension 915 mm × 205 mm × 6.35 mm were used as substrates for the depositions. Aluminum alloy AA6061 (AlMg1SiCu) in a T6 temper was used as the material both for the feedstock and substrate. The material's temperature-dependent material properties are summarized in Figure 3.
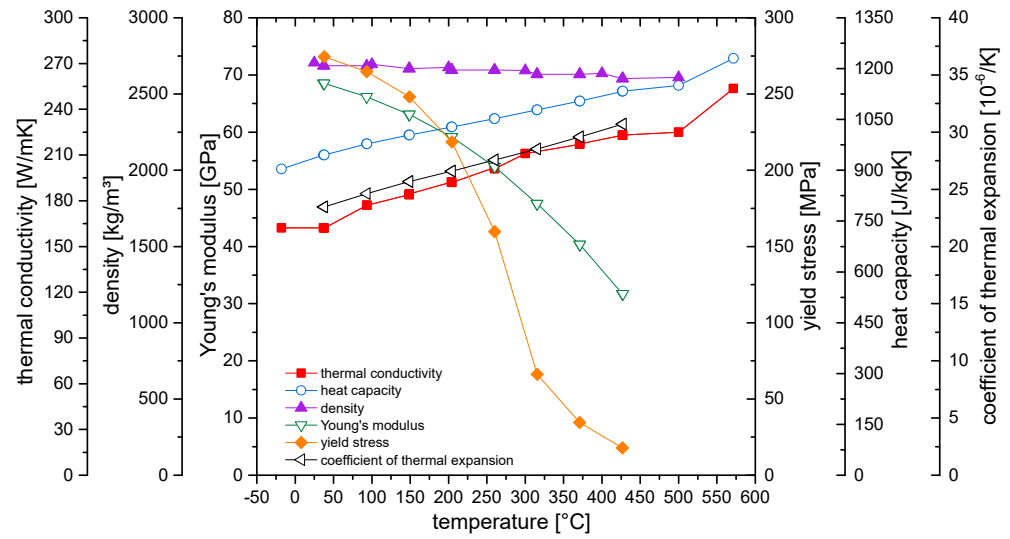
Figure 3. Temperature-dependent thermal and mechanical properties of AA6061-T6 from [10].

3.2. Tooling: Die Material, Geometry, and Properties

All dies for this study were made out of a H13 (1.2344/X40CrMoV5-1/SKD61) tool steel-hardened to 48–52 HRC (≈490–550 HV). H13 was chosen since this material offers excellent wear resistance, good thermal shock resistance, and high heat toughness [11], as is required for AFED. From the material, the blanks were machined, which included the common basic features needed for mounting the die on the spindle and for capturing and draining any material overflow out to the sides, see number 8 in Figure 1.

4. Experimental Setup and Procedure

The deposition tooling was mounted on an MTI LS-1 machine, which had been fitted with an extended retractable pin axis by Bond Technologies, as shown in Figure 1. This axis is used in the early-stage experimental setup to push the feedstock along and through the axis of the spindle. Additional tooling in the form of a guide tube, push rod, and tool holder, was also required for the AFED process.

All samples were built on the base plate, which was, therefore, fixed from the top and sides, Figure 4. The base plate was used in the "as-is" condition without any preconditioning, e.g., machining the surface or oxide removal. Different sample-build geometries were used at the different stages of the development process. Initially, straight 150 mm long lines were created, which enabled parameter changes during traversing. Once the initial parameters for a setup showed good extrusion results, a more representative 3D build geometry was used. This was a six-layer-high cylinder with an outer diameter of 60 mm and a 15–20 mm track width. This provided a long layer length and a substantial deposition time in a small area, creating real process conditions (temperature build-up, etc.) and allowing for the development of the parameters for a layer change. Finally, a full-size sample component was built for one selected tool, as described in Section 5.3.

During each experimental run, some of the feedstock seeped between the inner surface of the die and the guide tube end. This material was removed with various hand tools to provide a clean die surface for the next deposition run. Testing was performed in consecutive, explorative stages to inform tool design and to test hypotheses on the impact of tool design changes.

Figure 4. Tool holder with cooling collar (red), mounted die (silver), and fixturing. Background: linear and doughnut-shaped test extrusions.

5. Results and Discussion

Three geometrical features of the die are most relevant to the active material flow and process forces during plastification, extrusion, and deposition; see Figure 2: the topography of the inner and outer circular faces of the die and the geometry of its extrusion channels. In order to investigate their respective effects, seven different tool design variants were assessed based on two main extrusion hole shapes, a "bowtie" and a "tri-hole" design. One important aspect of the extrusion hole design was the inclination of the holes with respect to the vertical axis of the die (0, 15, or 45 degrees). For the topography of the inner and outer circular faces, the most important variation was the use of "scrolls", spiral grooves in the die that capture, transport, and consolidate the material toward the center, and "scoops", indentations that capture and move material axially through the die. Similar geometric features for inducing an active material flow are known from other solid-state processing techniques, such as Friction Stir Welding or friction extrusion. An illustrated summary of the basic designs (# 1 and # 2) and all their variants is presented in Figure 5, and Table 1 summarizes the die designs.
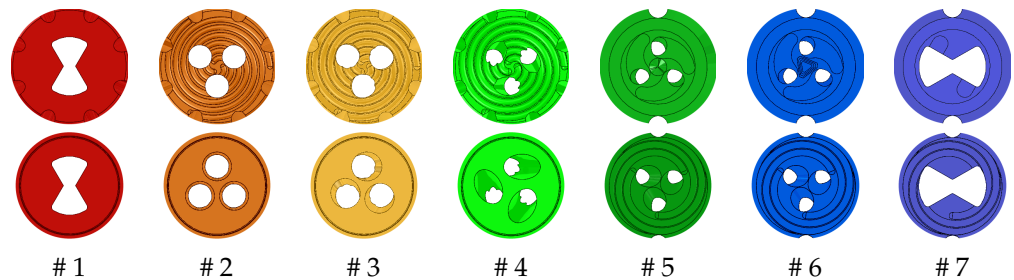
Figure 5. Designs of the inner (**top**) and outer (**bottom**) working surfaces of the seven different die designs tested showing material flow and extrusion features.

Table 1. The differences between die designs are based on their geometrical features. For images of the die working surfaces, see Figure 5.

| Die #	1	2	3	4	5	6	7
Extrusion passage	Bowtie	3 x	3 x @ 15°	3 x @ 45°	3 x/cone	3 x/pyramid	Bowtie
Inner surface	flat	scroll	scroll	scroll	scoop	scoop	flat
Outer surface	flat	flat	flat	flat	scroll	scroll	scroll
Overflow ejection	8 x	8 x	8 x	8 x	2 x	2 x	2 x
Hole Area mm^2	95	85	88	68	42	42	124
Hole Perimeter mm	46	57	58	52	40	40	53

5.1. Evolution of Tool Design

The original die designs # 1 and # 2 were derived from assessing the working principles of AFED, analogies to other solid-state processing techniques, and preliminary experimental work [6]. The most important aspect was to provide basic designs that allowed for the investigation and assessment of as many different development directions as possible. For example, die design # 1 has one continuous extrusion hole that includes the center of the die, which results in a direct "pass-through" effect of the rod force onto the substrate. In contrast, die design # 2 has three individual extrusion holes outside the die center, which effectively prevents such an effect. The first experimental stage tested the two basic die designs, # 1 and # 2, and determined that only a thin layer of feedstock was plasticized against the inner surface of the die. The dies scraped this extrudate off the end of the feedstock as a continuous ribbon, as shown on the left in Figure 6. In order to enhance this scraping effect, two new tri-hole die designs (# 3 & # 4) were created where the holes were machined at an angle to the surface of the die to provide a positive rake to the holes, see Figure 6 on the right.

Figure 6. Ribbon formation (extrudate), as generated by two different die designs: bow-tie # 1 (**left**, end of the rod with visible bulging) and 45° tri-hole # 4 (**right**, still within a die).

Dies # 3 and # 4 showed clearly improved material throughput and improved layer consolidation during deposition. This directly resulted in greater bead width and thickness capabilities. The increased deposition rate of these tools also allowed for deposition lengths of 750 mm, although the feedstock would eventually bind in the lower end of the guide tube. After die designs # 1, # 2, # 3, and # 4 had been tested, both the guide tube end design and the die shape were revised. The target was to reduce the amount of material overflow to the sides. This unwanted overflow occurred, especially during failed trials, and resulted in the need for extensive cleaning of the equipment. In order to reduce the overflow, the relief taper was changed from a square to a circular profile. Additionally, all subsequent die designs included more extensive geometrical features on the inside to capture and guide the material flow toward the extrusion holes. An illustrated description is provided in Figure 7.
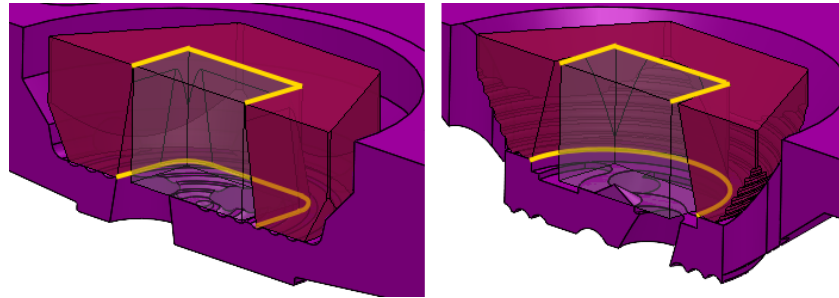
Figure 7. Initial (**left**) and revised (**right**) guide tube end/die interface. The initial design had a square taper, which allowed feedstock material to easily be forced between the die and guide tube end. The revised design had a transition from a square top to a circular bottom. Both contours of the taper (square and circular) are highlighted in yellow.

Dies # 5 and # 6 were both based on the tri-hole design and had a feature added to the center of the inner surface. This was carried out in an attempt to increase the thickness of the plasticized zone above the die and to guide the material directly to the three extrusion holes to improve the deposition rate, and this reduced the force on the feedstock. For die # 5, the feature was a smooth cone that was 1.3 mm high, and for die # 6, the feature was a stepped pyramid 2 mm in height. The scrolls on the inner face were replaced by deeper scoops to improve the flow into the extrusion holes. Additionally, scrolls were added to the outer face of the die to encourage a more extensive consolidation of the bead and to improve heat generation while keeping forces on the substrate low. Die # 7, the final design of this study was based on the bow-tie extrusion hole design. It also featured scoops on the inner surface and scrolls on the outer face of the die for the reasons stated above. Compared to the base design, # 1 it also featured a larger extrusion hole to align better with the size of the feedstock and the changes to the guide tube end and die shape described in Figure 5.

5.2. Quantitative Results for Tool Designs

During each deposition run, various parameters, such as spindle torque, feed force, substrate force, tool temperature, etc., were logged at about 50 Hz. The post-deposition analysis of these log files enabled quantitative comparisons of the elements of the die performance. For the following assessments, only those deposition runs that reached a stable, steady state were considered.

5.2.1. Process Efficiency and Process Window

An important quality characteristic of each die design is the specific energy required to deposit material, see Equation (9). Dies that require less energy per amount of material deposited are more efficient and are probably more effective at transporting material through the die. Figure 8 gives an overview of the specific process energy consumption and volumetric deposition rate for all die designs. In the figure, only deposition runs longer than 40 s were included, ensuring that die and process parameters were capable of maintaining the deposition process. The first 30 s and the last second of each log file were trimmed to ensure steady-state values.

From Figure 8, the specific process energy consumption is shown to be inversely correlated with the deposition rate in general. That is, as the deposition rate is increased, less energy is needed to deposit the same material volume. When reviewing Equation (9), $P_{heating}$ and $P_{deformation}$ have to scale linearly with $\dot{m}_{material}$, assuming the same processing conditions for the material. However, P_{losses} will largely scale with time and are more or less independent of the deposition rate. Together, this leads to the $\frac{1}{x}$ curve shown, and the magnitude of the effect shows that P_{losses} is a significant fraction of the process energy, especially at lower deposition rates. Furthermore, it is clear that with increasing volumetric deposition rate, the curve flattens out. This is because a minimum amount of

energy ($e_{process(theoreticalminimum)}$) is needed to establish AFED's working principle, i.e., the heating up, deforming, and depositing of a specific amount of material.
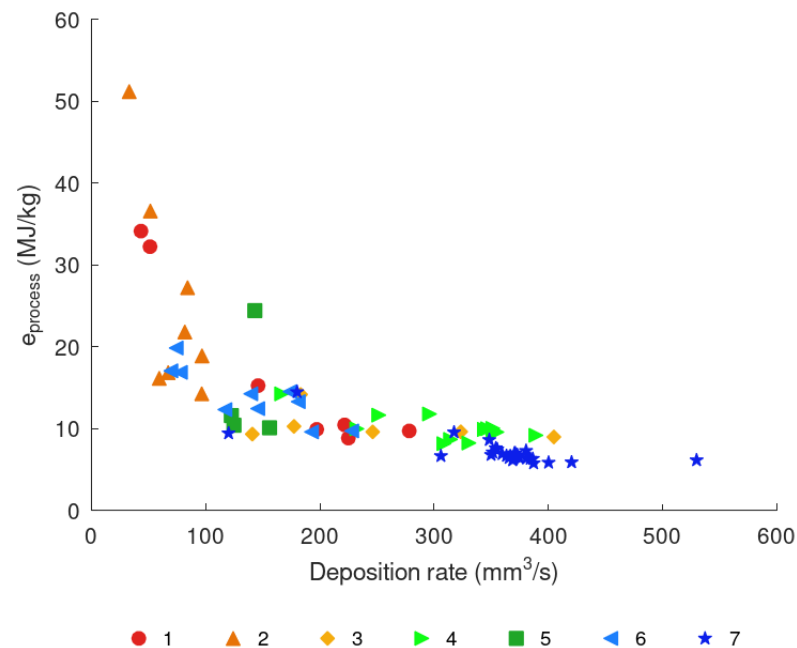
Figure 8. Specific process energy consumption (Equation (9)) by die number (see Figure 5) and volumetric deposition rate. The values are the averaged per deposition run during steady-state conditions.

From Figure 8, it is also clear that the efficiency of the various dies differs significantly. In particular, the initial designs # 1 and # 2 were not as capable of higher deposition rates and process efficiencies as the later designs # 3, # 4, or # 7. However, two of the later die designs # 5 and # 6 were found to be rather inefficient.

Two design factors can be identified and differentiated for this discussion: the ratio/area of the extrusion channel and the use of active material flow structures for extruding the feedstock.

As an example of the impact of active material flow structures, a direct comparison of dies # 2 and # 3 is useful. The only difference between the two is the active material flow structure implemented by an angle of the extrusion channels of 15° for die design # 3, see Table 1. As seen from Figure 8, the implementation directly enhances the process window and efficiency compared to the original die design. This impact is confirmed when comparing designs # 3 and # 4 with angles of 15° and 45°, respectively; they both show very similar capability and efficiency, although die design # 4 has over 30% more extrusion channel area.

In order to discuss the impact of larger extrusion channels, a comparison of the design of dies # 5 and # 6 with die # 3 is instructive. While having extensive inner and outer structures, dies # 5 and # 6 do not perform as well as the less structured design of die # 3. This is clearly because # 5 and # 6 only have half the extrusion hole area (42 mm²) of die # 3 (85 mm²), leading to a bottleneck and high forces inside the tooling, as described in the next section. However, it should be noted that due to the effect of active material flow structures, the performance of dies # 5 and # 6 is comparable to die design # 2, which has almost twice the extrusion channel area (but no angle). The most capable die design of this work with regard to deposition rate, die # 7, incorporates both: extensive inner and outer active material flow structures and a large area for the extrusion channel.

5.2.2. Feedstock Forces

Another good way to evaluate different tool designs and their ability to provide an efficient AFED process is to compare the inner forces required to achieve a given deposition rate. As described earlier, one of the ultimate goals of AFED is to reduce the forces acting on the substrate to a minimum. While the plasticizing and heating forces should ideally be fully compensated within the tool, it is still beneficial to keep these forces as low as possible; high forces can cause excessive overflow, rod bending, and die clogging and are a clear sign that the material is not being processed and extruded efficiently by the tool. Moreover, the machine's force capabilities are limited.

While the external deposition forces are heavily influenced by process parameters or conditions, such as the chosen layer height, part geometry, etc., the internal forces are more or less constrained by die geometry and the interaction of the die, guide tube, and feedstock. Figure 9 gives an overview of the rod forces for the seven die designs and different deposition rates. In comparison to the specific process energy consumption, a more clearly differentiated picture between the individual dies is evident. The rod force values of the individual dies tend to be grouped together (with varying scatter), which supports the conclusion that there is a die-specific force level in the steady state for each die that is almost independent of the deposition rate.
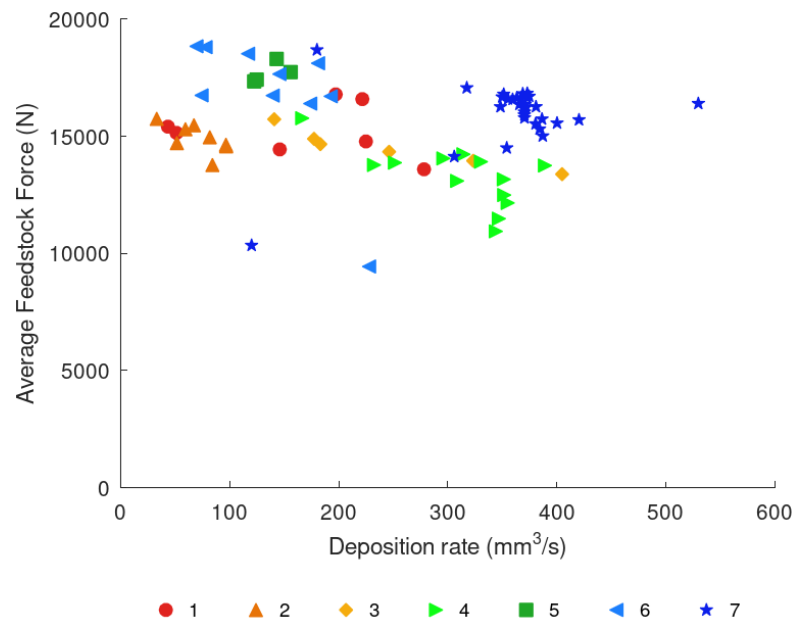
Figure 9. Feedstock forces by die number and volumetric deposition rate. Values are the averaged per deposition run during steady-state conditions.

It is also noteworthy that there is a clear tendency for dies with larger extrusion channels or more extensive geometric structures to have lower rod forces. For example, dies # 1 (95 mm² channel area), # 2 (85 mm²), and # 3 (88 mm²) show significantly lower forces, averaging around 15 kN, than dies # 5 and # 6 (both 42 mm²), which typically exceed 18 kN. This effect can be directly related to the reduction in the cross-sectional area of the flow channels, resulting in a higher pressure required to force the material through the die to achieve a comparable deposition rate.

It is also interesting that die # 4 has significantly lower rod forces than die # 7 (on average 12.5 kN to 16.5 kN) despite the fact that die # 7 has approximately 40% more extrusion channel area (# 4: 88 mm² and # 7: 124 mm²). This can be directly attributed to the material flow enhancing structures for vertical transport in the outer/substrate direction, which # 4 has but # 7 does not. The effect of these flow structures can be quantified using the design evolution of dies # 2, # 3, and # 4:

Die # 2 with three holes but no active material transport to the outside requires just over 15 kN on average. Die # 3 has a 15° angled flow enhancing structure, which reduces the force by approximately 0.5 kN, and # 4 with a 45° structure has the force reduced by approximately by 2.5 kN.

5.2.3. Substrate Forces

Ultimately, the most relevant criteria for AFED from a manufacturing perspective are the outer forces of the process acting on the substrate during deposition. With the perfect compensation of all the forces required to heat and plasticize the feedstock within the tool, the only forces acting on the substrate would be from the material flow to the outside and onto the substrate. By adjusting parameters such as layer height, spindle speed, or channel geometry, these forces could be kept to the minimum required for bonding to the substrate.

Figure 10 gives an overview on the force on the substrate by die number and volumetric deposition rate. By examining the average substrate force over all dies (which have the same outer diameter), an almost linear relationship between deposition rates and forces can be identified. This relationship is in good accordance with other solid-state processing technologies, such as Friction Stir Welding (FSW). At deposition rates below 100 mm^3/s, the force on the substrate is generally kept below 2 kN at 200 mm^3/s, mostly below 4 kN, etc. When averaged over all tools, this gives a slope of just over 20 Ns/mm^3, which can be interpreted as the impulse required to deposit 1 cubic millimeter of material on the substrate. This relationship can also be used to make statements about the process and local conditions; since all dies have the same outer diameter and only the successful depositions were considered, it can be concluded that this relationship follows the specific minimum thermo-mechanical process impact required for bonding to the substrate. As the local temperatures during the deposition runs were very homogeneous, this can be further reduced to the minimum mechanical process impact, i.e., the local contact pressure.

When comparing the substrate forces of the different die designs, it is striking that the two most efficient designs in terms of deposition rate, dies # 4 and # 7, are at similar levels despite their significantly different geometries. Die # 7 shows slight advantages in terms of throughput and die # 4 in substrate forces. The latter is particularly interesting, as die # 4 had already shown lower internal (rod) forces than # 7. The additional advantage of external forces can be attributed to the small direct passage in the center of die # 7, which allows a portion of the rod force to act almost directly on the substrate. This is not the case with die # 4, where the 45° angle of the extrusion channel does not allow direct passage but creates an additional vertical force component dependent on spindle speed. In this context, a direct comparison of dies # 3 and # 4 is, again, useful. As mentioned, the only difference between the two dies is the angle of their extrusion channels: 15° and 45°.

The greater ability of die # 4 to reduce internal forces compared to die # 3 has already been described. In the case of the external forces, the reverse is true: at less than 4 kN, die # 3 shows significantly lower substrate forces than die # 4, even at high deposition rates above 400 mm^3/s. In contrast, at over 8 kN, die # 4 is about 100% higher. Due to the small geometric differences, this effect can clearly be attributed to the differently induced vertical force components of the two dies. It also highlights the usefulness of the AFED operating principle in reducing the force on the substrate and the direct exchange of internal and external forces.

In direct comparison to die designs # 3 and # 4, , there is another interesting point to discuss. Although die # 2 was not capable of achieving higher deposition rates, the design, (which has neither a small direct passage like dies # 1 and # 7 nor an actively induced vertical material flow like dies # 3, # 4, # 5, and # 6) highlights the low substrate forces required by AFED, for example, for a deposition rate of around 100 mm^3/s, runs with less than 500 N substrate force are possible.
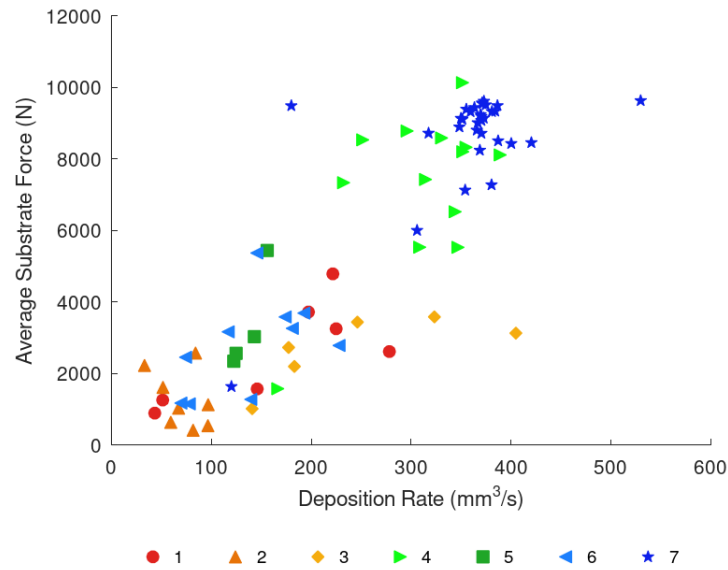
Figure 10. Force on the substrate by die number and volumetric deposition rate. Values are averaged per deposition run during steady-state conditions.

5.3. Sample Component

Among the tool designs tested, die # 7, the larger bow-tie design with internal and external material flow features, gave the most consistent and reliable deposition and showed the least material overflow. This design was, therefore, selected to demonstrate the basic capability of AFED for industrial manufacturing by building a full-size sample component, a square ring 300 mm × 300 mm × 50 mm, see Figure 11. The base plate for the build was 305 mm × 305 mm × 9.5 mm and was fastened to the machine table with 4× M 12 button head screws in a centered 200 mm × 200 mm pattern. In order to form a base, the first three layers of the build were run as single passes with variable heights ranging from 1.5 to 0.5 mm. Two 1 mm high layers were then deposited per deposition run, which equals a full rod of feedstock. Since the experimental machine setup did not have a continuous feed system, 25 individual runs were required to produce the full 50 mm height of the sample component. It was possible to process almost the entire rod without changing process conditions, such as rod forces. However, to ensure stable conditions, a few millimeters of rod were left in the guide tube for each run. Between the runs, the die was removed, cleaned, and a new rod inserted before the die was re-installed. The first layer of each run was produced at 500 rpm, while the second layer was produced at 400 rpm, as less heat was required. The layer width was set at 20 mm and remained consistent throughout the height of the build.

Figure 11. Completed sample component with base plate after the deposition process. Tensile specimens were extracted from the positions indicated in red.

5.4. Material Flow Analysis Based on Macros

For assessing microstructure and material flow during AFED, transverse and longitudinal macros were used. All macros were vibratory polished and then electrolytically etched using Barker's reagent. Figure 12 provides an overview of the structure and microstructure of the sample build, featuring the upper 14 layers. From the section shown, it is clear that the layers are fairly uniform with a homogeneous thickness and a similar microstructure. The individual layers can be clearly distinguished from each other and are macroscopically well-consolidated. With similarities to Friction Stir Welding (FSW) [12], the side where the traverse and rotational velocities are in the same direction (advancing side, left) demonstrate a more extensive material flow than the retreating side (right), where the rotational and linear process velocities are opposing. Consequently, and in line with FSW, the advancing side is much more sharply defined than the retreating side, which has a much rougher outer surface. This rougher outer surface is also associated with the presence of voids on the retreating side. These voids are embedded between banded, wavy, and periodic flow structures. These banded material flow structures are well known from the material flow characteristics of the FSW process [13].
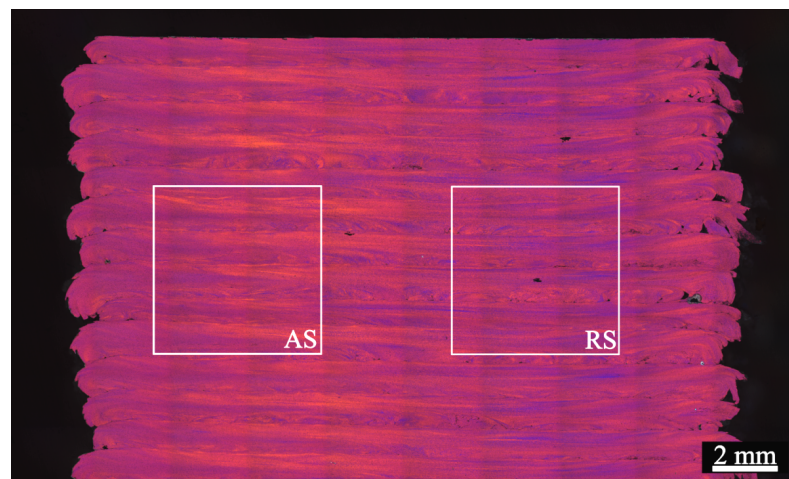
Figure 12. Cross-section in traverse direction showing the upper 14 deposited layers of the sample build (electrolytic Barker etching). Advancing side on the left; retreating side on the right.

When examining any layer in isolation, it is evident from the microstructure that the lower half of each deposited layer is not as strongly intermixed as the upper half. Some "cold shuts" and voids are visible in some of the layers' lower half at the transition to the preceding layer, again, mostly on the retreating side. Figure 13 provides a detail highlighting this. This can be attributed to the fact that this upper half is in direct contact with the spinning die during deposition and, thus, experiences higher levels of post-extrusion mechanical mixing, shearing, and thermal impact.

The longitudinal sections confirm the analysis of the transverse cross-sections: here, it can be seen that the flaws and inhomogeneities occur mainly in the layers that were created at the lower spindle speed level of 400 rpm, i.e., in every second layer of the build, Figure 14 (right). In those layers, banded structures of the periodic material flow are clearly recognizable, especially in their respective lower half. In the layers in between, carried out at 500 rpm, the material flow is far better consolidated. Here, the individual banded structures can often not be distinguished, and the overall process impact seems to be higher and more suitable for joining to the preceding layer.
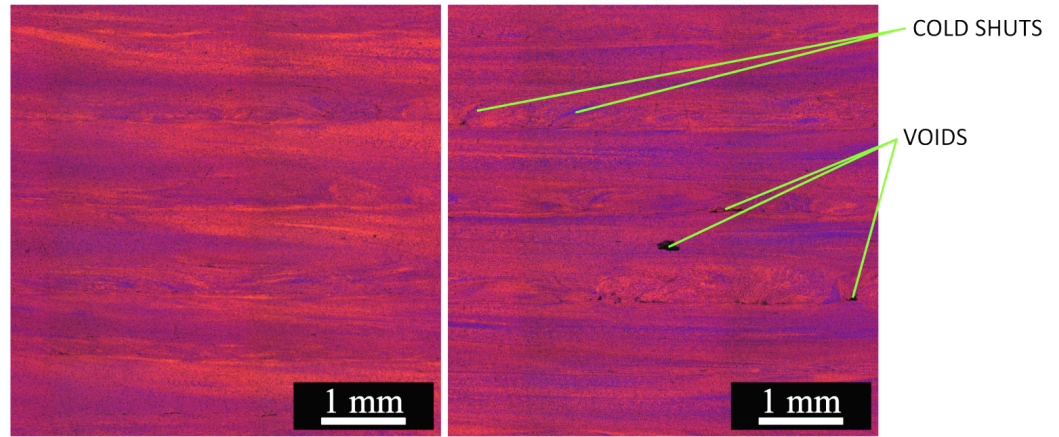
Figure 13. Macros of advancing (**left**) and retreating side (**right**). Locations, as marked in Figure 12.

Another characteristic of the AFED process can be recognized from the longitudinal sections. Analogous to Friction Stir Welding, a periodicity of the material flow can be identified in the layers, as shown in Figure 14. The banded structures, as found in the layers in Figure 14 created with a spindle speed level of 400 rpm, show a medium spacing, *d*, of about 1.42 mm. This corresponds well to what is to be expected from the two-fold symmetry of the tool's extrusion channels (bow tie), a 1,092 mm/min traverse speed and the spindle speed:

$$d = \frac{v_x}{2 \cdot \omega} = \frac{1092\,\text{mm/min}}{2 \cdot (400\,\text{rev/min})} = 1.365\,\text{mm} \tag{11}$$

It can be assumed, on the basis of the similarity to the FSW process, that the variance in the spacing of the banded structures (ranging from 1.354 to 1.467 mm) can be attributed to the tooling run-out or the asymmetry of the tool geometry, e.g., the orientation of the extrusion channels relative to the substrate when depositing.
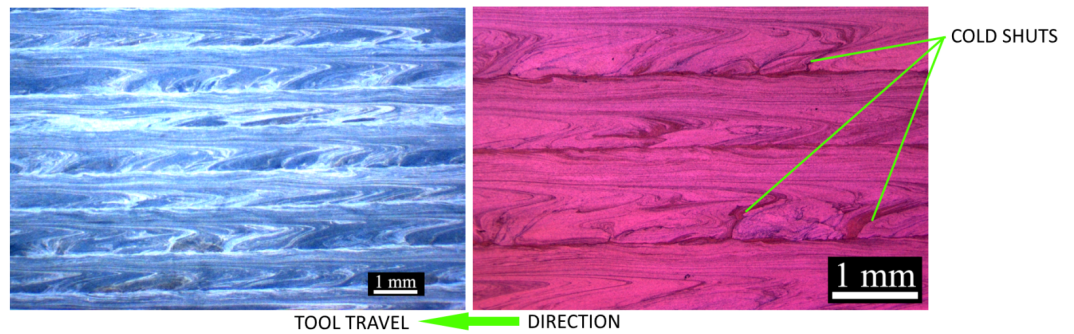
Figure 14. Left: Longitudinal overview along the traverse direction of the tool showing several deposited layers, coherence, and banded structures. **Right**: Longitudinal detail of the layers on the retreating side with magnification of the spacing and flaws. Tool travel direction is to the left.

5.5. Mechanical Testing and Properties

Tensile tests for this study were performed according to ISO 6892-2:2018. Round tensile specimens measuring $5 \times 25 \times 51$ were used (DIN 50125, Form B). All specimens were taken from the center of the layer and from the locations of the sample component, as sketched in Figure 11. The aim was to test both for the strength within the layers as well as for the bonding between them, i.e., in the horizontal and vertical (build) direction. The tests were carried out 6 months after the build to avoid any significant influence from the precipitation kinetics of the alloy [14].

Figure 15 shows the tensile test curves for the specimens. It can be seen that, within the elastic region and up to a plastic strain of some percent, specimens of both directions show very comparable behavior: Specimens in the vertical direction, Y2 and Y3, both reach a

yield stress of 138 MPa, and horizontal specimens X1 and X3 reach slightly higher values with 147 and 140 MPa. In the plastic region, the behavior begins to differ: the specimens in the build direction (vertical) fail in a brittle manner at plastic strains of only around 5% with ultimate tensile stresses of 189 and 185 MPa. The specimens along the layers (horizontal) show a significantly higher ductility of more than 20%, reaching 213 and 212 MPa. The behavior of the material in the horizontal direction corresponds closely to a T4 temper of the AA 6061 alloy, which is typical for extensive friction (stir) processing of age-hardenable alloys in T6 temper [12,15].
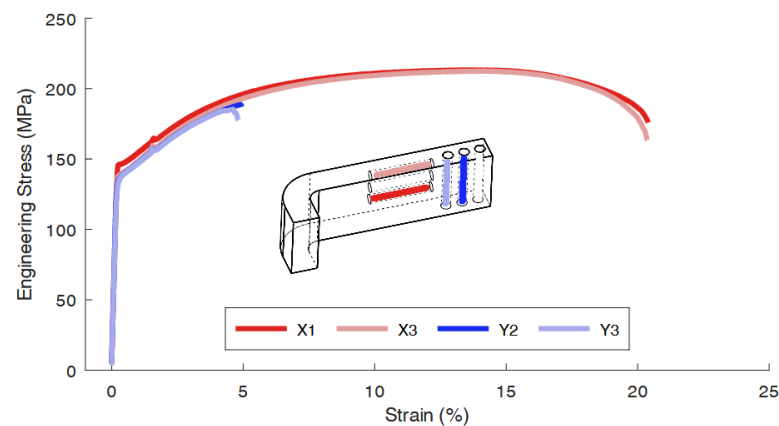
Figure 15. The stress/strain curves for tensile testing on the specimens and sketch with their respective extraction locations. Specimens X2 and Y1 (white) were damaged during sample preparation.

From the microstructural results presented earlier, the reason why the vertically oriented specimens experience brittle failure at lower stresses can be directly related to the flaws and inhomogeneities between the layers. With the onset of plastic deformation, the influence of internal notches becomes more relevant, acting as internal stress concentrators, which leads to crack initiation. Due to the focus of this work on industrialization, processes, and tool design, and the fact that extensive fractographic investigations have already been carried out for AFED in a recent study [6], a detailed fractographic investigation has been omitted at this point.

6. Summary

The target of this work was to contribute to the knowledge and state-of-the-art of additive friction extrusion deposition (AFED) through a comprehensive analysis of its working principles and an extensive experimental validation program.

As a first step, the working principle and AFED's process mechanics were broken down into their individual components. Inner and outer forces, their origins and impact on the process were described. Based on this, the energy equations of the process and different measures for process efficiency were derived and the theoretical minimum energy consumption of the process was described. Together, these analytical results form the basis for all further process optimizations as the experimental program of this work.

Three geometrical features of the extrusion dies were identified as most relevant to the active material flow, the process forces, and deposition quality: the topography of the inner and outer circular faces and the geometry of its extrusion channels. For investigating their respective effects, seven different tool design variants were assessed. The experimental program demonstrated the importance of the inner structures both for heating up and plasticizing as well as guiding and transporting the plasticized material to the extrusion channels. Dies designed accordingly showed extended process envelopes, higher throughputs, and less tendency for material overflow. The experiments proved that it is possible to exchange outer (substrate) forces for inner forces and, therefore, validated AFED's central idea of reducing substrate forces by the separation of forces needed for plasticizing and deposition. The experiments showed that AFED is capable both of high material throughput (near

550 mm³/s) and also of reducing the substrate forces: For example, the forces for a run at 100 mm³/s remained below 500 N, and for a run at 400 mm³/s below 3500 N.

Based on the macros of the sample component, the microstructure was assessed and the material flow in AFED was characterized. It was shown that the advancing and retreating side of the process differ significantly both in material flow and the resulting microstructure. As in FSW, the advancing side was found to have a higher process impact than the retreating side. The advancing side was, therefore, much more sharply defined than the retreating side, which, in addition, showed a much rougher outer surface. The banded material flow structures were found in the macros, a phenomenon known from other solid-state processing techniques. These structures are indicative of a periodic material flow that is additionally influenced by the external structures of the die as extrusion channels. The macros also underlined that a minimum thermal and, especially, mechanical process, impact is needed to ensure effective layer-to-layer bonding. In mechanical testing, bonding flaws between layers resulted in more brittle failure behavior in the build direction, while in the horizontal direction of the build, mechanical properties corresponding to a T4 temper were achieved.

The manufacturing of the sample components demonstrated that AFED is already capable of producing industrial-grade components. However, the study revealed several further areas of possible improvements both for process efficiency and build quality. The greatest potential for optimization lies in the processing strategy and, thus, in the field of die design. For some dies, especially # 3, a good balance between inner and outer forces and also the heating of the material was achieved. However, a design strategy that balances inner and outer heating better still has to be formalized. The material has to be heated up within the die just enough to be softened and plasticized and able to flow through it. Extrusion channels and also outer structures should take care of the remaining thermo-mechanical impact needed for consolidation and bonding to the preceding layers. Heating the material up too much within the die will cause overheating it during the extrusion and deposition process. In addition, overheating the material will cause significant heat to flow back into the feedstock, making the process inefficient and favoring material overflow and feedstock binding.

The other important area of improvement is layer-to-layer bonding. As shown by the experiments presented here, a minimum local pressure is needed for a good bonding. In order to keep the forces low during deposition, improved designs and processing strategies are needed that reduce the contact area or implement higher pressures only very locally, close to the trailing edge of the tool. Techniques from technologies such as FSW provide promising approaches, e.g., additional spirals on the outer surface or tilting the spindle.

contribution of the University of Michigan, namely Pingsha Dong and Adbul Sayeed Khan, for their fundamental work with SoftTouch AM™ technology.

References

1. Rivera, O.G.; Allison, P.G.; Jordon, J.B.; Rodriguez, O.L.; Brewer, L.N.; McClelland, Z.; Whittington, W.R.; Francis, D.; Su, J.; Martens, R.L.; et al. Microstructures and mechanical behavior of Inconel 625 fabricated by solid-state additive manufacturing. *Mater. Sci. Eng. A* **2017**, *694*, 1–9. [CrossRef]
2. Griffiths, R.J.; Perry, M.E.J.; Sietins, J.M.; Zhu, Y.; Hardwick, N.; Cox, C.D.; Rauch, H.A.; Yu, H.Z. A Perspective on Solid-State Additive Manufacturing of Aluminum Matrix Composites Using MELD. *J. Mater. Eng. Perform.* **2019**, *28*, 648–656. [CrossRef]
3. Jordon, J.B.; Allison, P.G.; Phillips, B.J.; Avery, D.Z.; Kinser, R.P.; Brewer, L.N.; Cox, C.; Doherty, K. Direct recycling of machine chips through a novel solid-state additive manufacturing process. *Mater. Des.* **2020**, *193*, 108850. [CrossRef]
4. Tuncer, N.; Bose, A. Solid-State Metal Additive Manufacturing: A Review. *JOM* **2020**, *72*, 3090–3111. [CrossRef]
5. Martin, L.P.; Luccitti, A.; Walluk, M. Evaluation of additive friction stir deposition of AISI 316L for repairing surface material loss in AISI 4340. *Int. J. Adv. Manuf. Technol.* **2022**, *121*, 2365–2381. [CrossRef]
6. Liu, F.; Dong, P.; Khan, A.S.; Zhang, Y.; Cheng, R.; Taub, A.; Ma, Z. 3D printing of fine-grained aluminum alloys through extrusion-based additive manufacturing: Microstructure and property characterization. *J. Mater. Sci. Technol.* **2023**, *139*, 126–136. [CrossRef]
7. Griffiths, R.J.; Petersen, D.T.; Garcia, D.; Yu, H.Z. Additive Friction Stir-Enabled Solid-State Additive Manufacturing for the Repair of 7075 Aluminum Alloy. *Appl. Sci.* **2019**, *9*, 3486. [CrossRef]
8. Hossfeld, M. Shoulderless Friction Stir Welding: A low-force solid state keyhole joining technique for deep welding of labile structures. *Prod. Eng.* **2021**, *16*, 389–399. [CrossRef]
9. Hossfeld, M. On Friction, Heat Input, and Material Flow Initiation during Friction Stir Welding: Tool and Process Optimization. *J. Manuf. Mater. Process.* **2023**, *7*, 34. [CrossRef]
10. Hossfeld, M. Modeling Friction Stir Welding: On Prediction and Numerical Tool Development. *Metals* **2022**, *12*, 1432. [CrossRef]
11. Tekmen, C.; Toparli, M.; Ozdemir, I.; Kusoglu, I.M.; Onel, K. High temperature behaviour of H13 steel. *Z. Für Met.* **2005**, *96*, 1431–1433. [CrossRef]
12. Hoßfeld, M. *Experimental, Analytical and Numerical Investigations of the Friction Stir Welding Process*; Universität Stuttgart: Stuttgart, Germany, 2016. [CrossRef]
13. Gratecap, F.; Girard, M.; Marya, S.; Racineux, G. Exploring material flow in friction stir welding: Tool eccentricity and formation of banded structures. *Int. J. Mater. Form.* **2012**, *5*, 99–107. [CrossRef]
14. Hossfeld, M. Time-dependency of mechanical properties and component behavior after friction stir welding. *Int. J. Adv. Manuf. Technol.* **2019**, *102*, 2297–2305. [CrossRef]
15. von Strombeck, A.; Dos Santos, J.F.; Torster, F.; Laureano, P.; Kocak, M. Fracture toughness behaviour of FSW joints aluminium alloys. In Proceedings of the First International Symposium on Friction Stir Welding, Thousand Oaks, CA, USA, 14–16 June 1999.